Microfluid Nanofluid (2013) 14:817–829
DOI 10.1007/s10404-012-1082-8

RESEARCH PAPER

Inertia effect on deformation of viscoelastic capsules in microscale flows

Bo Feng Bai · Zheng Yuan Luo · Shu Qi Wang · Long He · Tian Jian Lu · Feng Xu

Received: 29 June 2012 / Accepted: 9 October 2012 / Published online: 16 November 2012
© Springer-Verlag Berlin Heidelberg 2012

Abstract The deformation of capsules (i.e., cells, bacterial) in microscale flows plays an important role in biofluid flows such as blood flow in capillaries and cell manipulation in microfluidics. In previous studies on capsule deformation in microscale flows, the inertia effect was often assumed to be negligible and thus omitted. However, this assumption may not reflect real situations, as indicated by recent studies of inertial microfluidics. As such, we aimed to study the inertia effect on capsule deformation in microscale flows and to determine under which conditions this effect may be omitted. Using a collocated grid projection scheme, we developed a finite difference-front tracking method, and investigated the deformation of viscoelastic capsules in microscale flows for Reynolds number (*Re*) ranging from 0.01 to 10 as seen in vitro and in vivo. The results showed that the transient and steady-state deformation of capsules was significantly affected by inertia, and the flow structure varied considerably when *Re* was varied from 0.1 to 10. No significant changes were found for *Re* ranging from 0.01 to 0.1, and hence the inertia effect on capsule deformation in the microscale flows can be omitted when *Re* is less than 0.1. These findings improve the current understanding of the mechanism underlying cell movement in capillaries and can be applied to optimize the conditions for cell manipulation and separation in microfluidic devices.

Keywords Inertia · Capsules · Deformation · Microscale flows · Microfluidics

B. F. Bai and Z. Y. Luo contributed equally to this work.

B. F. Bai (✉) · Z. Y. Luo · L. He
State Key Laboratory of Multiphase Flow in Power Engineering, Xi'an Jiaotong University, Xi'an 710049, People's Republic of China
e-mail: bfbai@mail.xjtu.edu.cn

B. F. Bai · Z. Y. Luo · T. J. Lu · F. Xu (✉)
Biomedical Engineering and Biomechanics Center, Xi'an Jiaotong University, Xi'an 710049, People's Republic of China
e-mail: fengxu@mail.xjtu.edu.cn

S. Q. Wang
HST-Center for Biomedical Engineering, Department of Medicine, Brigham and Women's Hospital, Harvard Medical School, Boston 02139, MA, USA

F. Xu
The Key Laboratory of Biomedical Information Engineering of Ministry of Education, School of Life Science and Technology, Xi'an Jiaotong University, Xi'an 710049, People's Republic of China

1 Introduction

Fluid flows with suspending capsules (i.e., cells, bacterial) are common in both biological processes and bioengineering microfluidics, such as blood flow in capillaries (Popel and Johnson 2005; McWhirter et al. 2009), cell migration and adhesion during inflammations (Ley et al. 2007), as well as cell manipulation and separation in microfluidic devices (Didar and Tabrizian 2010). For flow occurring at a microscale level, the deformation of capsules becomes extremely important for flow characteristics. For example, the high deformability of red blood cells renders them the capability to flow through capillaries (Eggleton and Popel 1998; Bagchi 2007), and the deformation of leukocytes increases their contact area with endothelial cells, strengthening cell adhesion to vascular wall (Dong et al. 1999; Jadhav et al. 2005; Luo et al. 2011a). Besides, cell sorting microfluidic devices have been developed

based on cell deformability (Beech et al. 2012; Hou et al. 2010; Hur et al. 2011). However, as the mechanisms underlying capsule deformation in microscale flows are not yet completely clear, the understanding of relevant biological processes and the development of bioengineering microfluidic devices are restricted. Investigations on the mechanisms of capsule deformation are therefore essential to further studies on biological processes and bioengineering microfluidics.

Since it is challenging to precisely control microscale flow conditions and image minute changes in experiments, theoretical modeling has been widely employed in capsule deformation studies (Ramanujan and Pozrikidis 1998; Pozrikidis 2001; Lac and Barthes-Biesel 2005; Yue et al. 2005b; Sui et al. 2007; Chung et al. 2008; Foessel et al. 2011; Luo et al. 2011b; Abkarian and Viallat 2008). However, the inertia effect on capsule deformation was often neglected, which may not reflect real situations of biological processes and bioengineering microfluidics. In fluid mechanics, inertia is defined as the resistance to changes of fluid motion, which is usually quantified by the Reynolds number *Re* (the ratio of inertial forces to viscous forces). As the Reynolds number associated with microscale flows is typically low (<1), inertia is generally assumed to have little or no contribution to microfluidic phenomena including capsule deformation (Di Carlo 2009). Further, accounting for the inertial effect on capsule deformation will remarkably increase the complexity of theoretical modeling. However, results from recent studies on inertial microfluidics indicate that inertia may affect fluid velocity around capsules in microscale flows, thus affect capsule deformation and migration (Di Carlo et al. 2007; Di Carlo 2009; Wu et al. 2009). For instance, inertia can significantly promote the deformation of Newtonian capsules (a Newtonian fluid surrounded by an elastic membrane) (Sui et al. 2009) and liquid drops (a Newtonian fluid without an elastic membrane) (Sheth and Pozrikidis 1995) for moderate Reynolds numbers (between 1 and 100). Since the Reynolds number in microscale flows in vitro and in vivo is often less than 1 (Stone and Kim 2001; Squires and Quake 2005), whether and when the inertial effect on capsule deformation may be omitted in microscale flows remains unknown.

In this study, we developed a mathematical model to investigate the conditions under which the inertial effect on capsule deformation in microscale flows may be omitted within the physiologically meaningful *Re* range of 0.01–10. To this end, a finite difference-front tracking method was employed, in which a collocated grid projection scheme was used to solve the full Navier–Stokes equations. Predictions from this model showed that the inertial effect on capsule deformation may be omitted only when *Re* was less than 0.1. This study provides new insights into microscale flows with suspending capsules, furthering the current understanding of biological processes and design of bioengineering microfluidic devices.

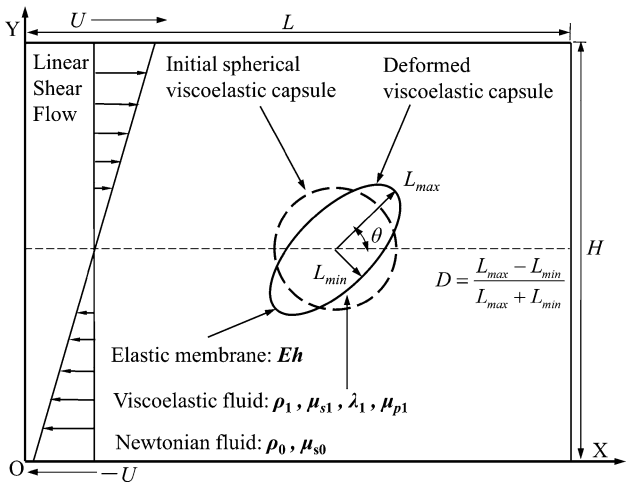

Fig. 1 Schematic diagram of viscoelastic capsule deformation under linear shear flow. The viscoelastic capsule was modeled as viscoelastic fluid (density ρ_1 and viscosity μ_1) surrounded by an elastic membrane (stiffness Eh). Surrounding fluid is Newtonian with density ρ_0 and viscosity μ_0. Deformation of the capsule is characterized by dimensionless deformation index D and orientation angle θ

2 Computational method

2.1 Flow configuration

With reference to Fig. 1, a linear shear flow was employed to investigate the inertia effect on capsule deformation, which has been extensively used in previous theoretical modeling of capsule deformation (Eggleton and Popel 1998; Ramanujan and Pozrikidis 1998; Lac and Barthes-Biesel 2005; Yue et al. 2005b; Chung et al. 2008; Foessel et al. 2011). An initially spherical viscoelastic capsule with radius R is placed in the center of a computational domain having length L and height H. The upper and bottom boundaries (plates) of the domain are moved in opposite directions with constant velocity U, generating a linear shear flow with shear rate $k = 2U/H$. The viscoelastic capsule is composed of a viscous fluid (density ρ_1 and viscosity μ_1) and the surrounding elastic membrane (stiffness Eh, E being the shear modulus of elasticity and h the thickness of the membrane). The capsule is immersed in a Newtonian fluid such as plasma of density ρ_0 and viscosity μ_0, and the fluid flow is taken as incompressible.

2.2 Governing equations

The incompressible fluid flow is governed by mass and momentum conservation equations, given by:

$$\nabla \cdot \mathbf{u} = 0 \tag{1}$$

$$\frac{\partial(\rho \mathbf{u})}{\partial t} + \nabla \cdot (\rho \mathbf{u}\mathbf{u}) = \nabla \cdot \boldsymbol{\tau} + \mathbf{F} \tag{2}$$

where $\mathbf{u}$ is the velocity vector, ρ and t are the density and time, $\mathbf{F}$ is the body force generated from the elastic membrane, and $\boldsymbol{\tau}$ is the total stress tensor calculated by:

$$\boldsymbol{\tau} = -p\mathbf{I} + \mu_s\left[\nabla \mathbf{u} + (\nabla \mathbf{u})^T\right] + \mathbf{T_p} \tag{3}$$

Here, p and $\mathbf{I}$ are the pressure and unit tensor, μ_s is the solvent viscosity (the Newtonian part of the fluid), and $\mathbf{T_p}$ is the extra stress tensor (or viscoelastic stress) from the non-Newtonian part, which is governed by the Oldroyd-B constitutive equation (Boger 1977; Bird and Wiest 1995):

$$\lambda\left[\frac{\partial \mathbf{T_p}}{\partial t} + (\mathbf{u} \cdot \nabla)\mathbf{T_p} - \mathbf{T_p} \cdot (\nabla \mathbf{u}) - (\nabla \mathbf{u})^T \cdot \mathbf{T_p}\right] + \mathbf{T_p} = \mu_p[\nabla \mathbf{u} + (\nabla \mathbf{u})^T] \tag{4}$$

where λ and μ_p are the relaxation time and polymeric viscosity of the non-Newtonian part. The total viscosity of the viscoelastic fluid is the sum of the solvent viscosity and the polymeric viscosity.

2.3 Numerical implementation

Initially, the spherical viscoelastic capsule is placed in the center of the computational domain, where the initial flow is a linear shear flow characterized by velocity field $\mathbf{u} = (ky - U, 0)$; see Fig. 1. Initially, zero value of the extra stress tensor $\mathbf{T_p}$ is set for the Oldroyd-B constitutive equation. Non-slip boundary condition is imposed at the upper and bottom boundaries. The slip lengths are reported experimentally in the range of molecular lengths to hundreds of nanometers (Lauga et al. 2007). It is appropriate to assume non-slip boundary conditions at solid–liquid boundaries when typical dimensions of systems are larger than tens of micrometers (Worner 2012). In our system, the typical dimension is 30–160 μm and thus it is reasonable to use the non-slip boundary condition. Periodic boundary condition is applied for x-direction (flow direction) boundaries. At all the boundaries of the computational domain, the fluid is Newtonian and the extra stress is always zero, and thus no special boundary conditions are needed for the extra stress.

The moving interface (i.e., the elastic membrane) is tracked using the front tracking method developed by Tryggvason and co-workers (Unverdi and Tryggvason 1992; Tryggvason et al. 2001). In this method, the velocity field and the extra stress of the two-phase flow (capsule and surrounding fluid) are solved by a single set of equations (i.e., Eqs. 1, 2 and 4), with changing properties across the interface (i.e., density, solvent viscosity, polymeric viscosity and relaxation time) similar to that in single-phase systems. An indicator function $I(\boldsymbol{x}, t)$, with value 1 inside the capsule and 0 outside, is constructed for the changing properties, as:

$$\phi(\boldsymbol{x}, t) = \phi_0 + (\phi_1 - \phi_0)I(\boldsymbol{x}, t) \tag{5}$$

where ϕ represents the changing properties including ρ, μ_s, μ_p and λ. The indicator function is obtained by solving the Poisson equation (Unverdi and Tryggvason 1992; Sarkar and Schowalter 2000) given below:

$$\nabla^2 I(\boldsymbol{x}, t) = \nabla \cdot \left[\sum_l D(\boldsymbol{x} - \boldsymbol{x}^{(l)}) n^{(l)} \Delta s^{(l)}\right] \tag{6}$$

where $\boldsymbol{n}^{(l)}$, $\boldsymbol{x}^{(l)}$ and $\Delta s^{(l)}$ are the unit normal vector, centroid and length of a discrete line segment l of the membrane, and D is the delta distribution function defined in Eq. 7. The elastic force on the membrane is distributed onto Eulerian grids and introduced as a source of body force using the distribution function as (Peskin 1977; Unverdi and Tryggvason 1992):

$$D(x - x') = \begin{cases} \frac{1}{4h}\left[1 + \cos\left(\frac{\pi(x - x')}{2h}\right)\right] & \text{for } |x - x'| \le 2h \\ 0 & \text{for } |x - x'| > 2h \end{cases} \tag{7}$$

where x' is the position of an arbitrary point on the elastic membrane and h is the Eulerian grid size.

To obtain the elastic force on the surrounding elastic membrane, the classical Hooke's law is employed as the constitutive equation of the elastic membrane for its simplicity and ability to effectively capture the general features of the capsule membrane (Jadhav et al. 2005). More complex constitutive equations for the membrane can be easily implemented into the present model. Then, the tension T_e on a one-dimensional (1D) elastic membrane in 2D simulation may be calculated as (Bagchi et al. 2005; Bagchi 2007):

$$T_e = Eh\left(\varepsilon^{3/2} - \varepsilon^{-3/2}\right) \tag{8}$$

where ε is a stretch ratio of undeformed length to deformed length of a line segment that connects two adjacent Lagrangian grid points on the membrane.

A second order projection method based on the collocated grid system is used to solve the governing equations. In this method, the solution procedure includes three steps, as follows:

$$\frac{\mathbf{u}^* - \mathbf{u}^n}{\Delta t} = \text{Convective}(\mathbf{u}^n) + \text{Stress}(\mathbf{u}^n) + \text{Bodyforce}(\mathbf{u}^n) \tag{9}$$

$$\nabla^2 p = \frac{\nabla \cdot \mathbf{u}^*}{\Delta t} \tag{10}$$

$$\mathbf{u}^{n+1} = \mathbf{u}^{*} - \Delta t \cdot \nabla p. \tag{11}$$

An intermediate velocity field $\mathbf{u}^*$ is first solved (Eq. 9) to decouple the pressure computation into the second step (Eq. 10). The velocity field in the next step $\mathbf{u}^{n+1}$ is then obtained by correcting the intermediate velocity field $\mathbf{u}^*$ using the pressure (Eq. 11).

The staggered grid system traditionally employed to ensure full coupling between pressure and velocity is complicated, since the pressure and velocity need to be calculated on different grid nodes. In contrast, with the collocated grid scheme, the pressure and velocity are calculated on the same grid nodes, thus much easier to be implemented than the staggered grid scheme. However, insufficient pressure–velocity coupling in projection methods using the collocated grid system may induce checkerboard oscillations and thus limit their application. To address this challenge, we developed a pressure-weighted interpolation instead of the traditional linear interpolation for fluxes interpolation that determines the pressure–velocity coupling, as:

$$\begin{aligned} F^{u}_{i+1/2,j} &= \frac{u_{i+1,j} + u_{i,j}}{2} - \Delta t \frac{p_{i+1,j} - p_{i,j}}{\Delta x} \\ F^{v}_{i,j+1/2} &= \frac{v_{i,j+1} + v_{i,j}}{2} - \Delta t \frac{p_{i,j+1} - p_{i,j}}{\Delta y} \end{aligned} \tag{12}$$

The projection method ensures a second order temporal accuracy for unsteady flow. The Crank–Nicholson semi-implicit technique is employed to update the diffusion term for stability, whilst the Adams–Bashforth method is used to update other terms including advection, pressure, body force and membrane advection equation. The pressure Poisson equation is solved by using the alternating direction implicit scheme and multi-grid techniques. The standard central difference scheme is employed to spatially discretize the governing equations except the constitutive equation. The first order upwind scheme is used to discretize the convective term of the constitutive term for convergence (Sarkar and Schowalter 2000).

2.4 Non-dimensionalization

The non-dimensional parameters include: Reynolds number $Re = \rho_0 kR^2/\mu_0$, dimensionless stiffness $G = \mu_0 kR/Eh$, Deborah number $De = \lambda k$, density ratio $\lambda_\rho = \rho_1/\rho_0$, solvent viscosity ratio $\lambda_{\mu s} = \mu_{s1}/\mu_{s0}$, ratio of polymeric viscosity to solvent viscosity for viscoelastic fluid inside the capsule $\beta_1 = \mu_{p1}/\mu_{s1}$. For simplicity and focusing on the inertia effect on capsule deformation, we fix $\lambda_\rho = \lambda_{\mu s} = \beta_1 = 1$. The Taylor parameters (deformation index D and orientation angle θ) are used to characterize the capsule deformation, with $D = (L_{max} - L_{min})/(L_{max} + L_{min})$ where L_{max} and L_{min} are the maximum and minimum axis of the capsule and θ is the angle between the maximum axis of the capsule and the x-axis (Fig. 1).

3 Results

3.1 Convergence and validation

In the previous section, a computational model based on a finite difference-front tracking method has been developed to investigate the inertia effect on capsule deformation in microscale flows. To ensure the accuracy of our code, a convergence study was implemented including eliminating the effects of computational domain size and grid resolution on capsule deformation. For this purpose, we tested three computational domain sizes ($L = H = 12R$, $16R$ and $20R$) and three Eulerian grid systems (10, 20 and 30 grids for one capsule having radius $1R$). The predicted temporal evolution of deformation index D and orientation angle θ for these three computational domain sizes and three grid systems was shown in Fig. 2. The steady-state deformation (D_s and θ_s) for capsule deformation attained small numerical errors: $(D_s^{20R} - D_s^{16R})/D_s^{16R} = 0.032$ %, $(\theta_s^{20R} - \theta_s^{16R})/\theta_s^{16R} = 0.63$ %, $(D_s^{30} - D_s^{20})/D_s^{20} = 0.13$ %, $(\theta_s^{30} - \theta_s^{20})/\theta_s^{20} = -0.41$ % at $Re = 1$, $G = 0.12$. Therefore, the computational domain size of $16R$ and Eulerian grid system of 20 grids for $1R$ were used for all later computations. Besides, the ratio of Lagrangian grid length to Eulerian grid length is fixed at 0.5 for all computations, which was validated to be sufficient for capturing important features of capsule deformation (Sui et al. 2009).

We next validated our model by comparing its prediction on capsule deformation with other theoretical modeling efforts. Firstly, the deformation of Newtonian capsule (a Newtonian fluid surrounded by an elastic membrane) in linear shear flow was simulated to validate the model for the elasticity of capsule membrane. The predicted steady-state deformation (D_s and θ_s) versus dimensionless stiffness G was compared with Breyiannis's (Breyiannis and Pozrikidis 2000) and Sui's (Sui et al. 2009) simulations (Fig. 3a). We predicted higher values of D_s than Breyiannis's results and lower values than Sui's results. But the largest discrepancy between our results and Breyiannis's as well as Sui's results was separately 4.6 and 2.8 % for all the range of G, which validated our code for the case of capsule membrane elasticity. To validate our code for the viscoelasticity of the fluid inside the capsule, we simulated the deformation of a viscoelastic drop (a viscoelastic fluid surrounded by an interface with constant surface tension σ) in Newtonian fluid matrix under linear shear flow. We compared our results with Chinyoka's numerical results (Chinyoka et al. 2005) for capillary numbers $Ca = 0.24$ and $Ca = 0.6$ ($Ca = \mu_0 kR/\sigma$), while keeping all other parameters (Re, Ca, λ_ρ, $\lambda_{\mu s}$, $\lambda_{\mu p}$ and β_1) equivalent to those used by Chinyoka. The time evolution of drop shape and deformation index D was accurately reproduced (Fig. 3b). The difference of deformation index D at $t = 3$ between our results and Chinyoka's was only 2.74 and 1.03 % for $G = 0.24$ and $G = 0.6$, respectively.

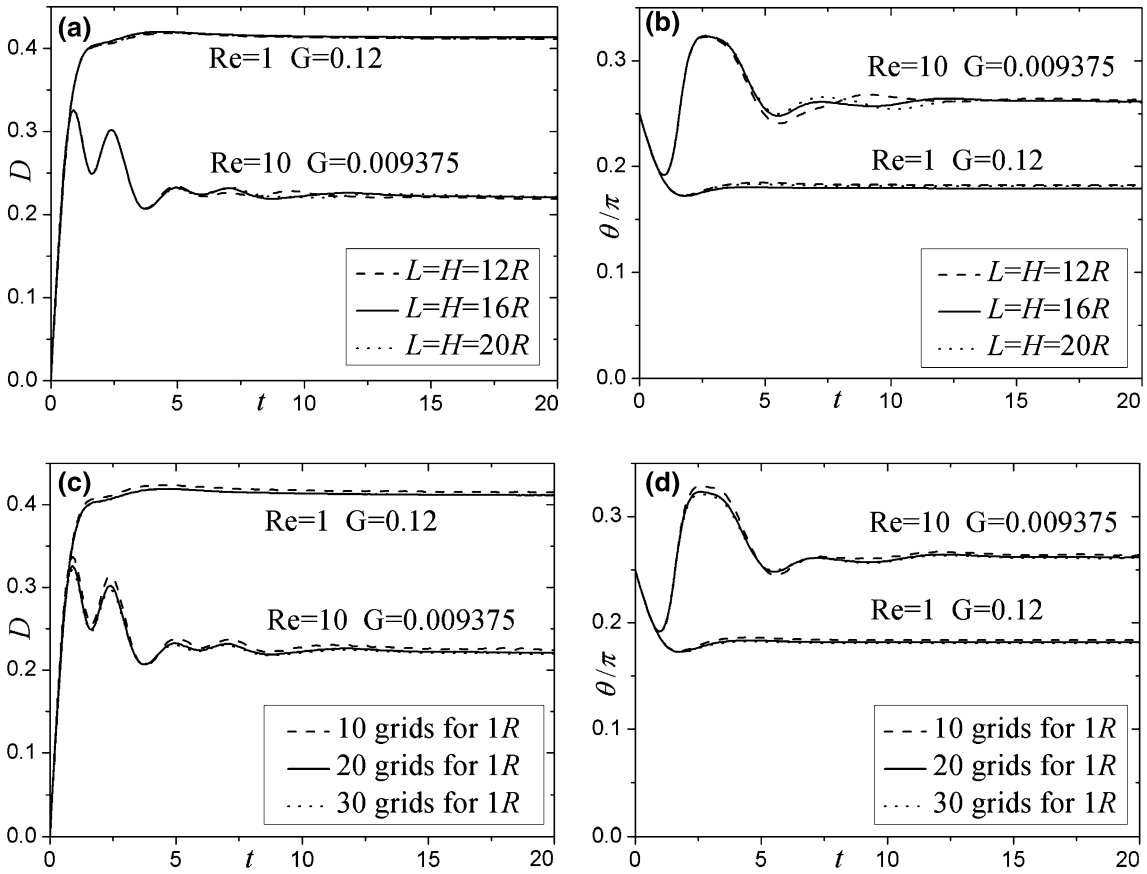

Fig. 2 Numerical performance. **a**, **b** is temporal evolution of deformation index D and orientation angle θ under various computational domain sizes; **c**, **d** is temporal evolution of deformation index D and orientation angle θ under various grid resolutions

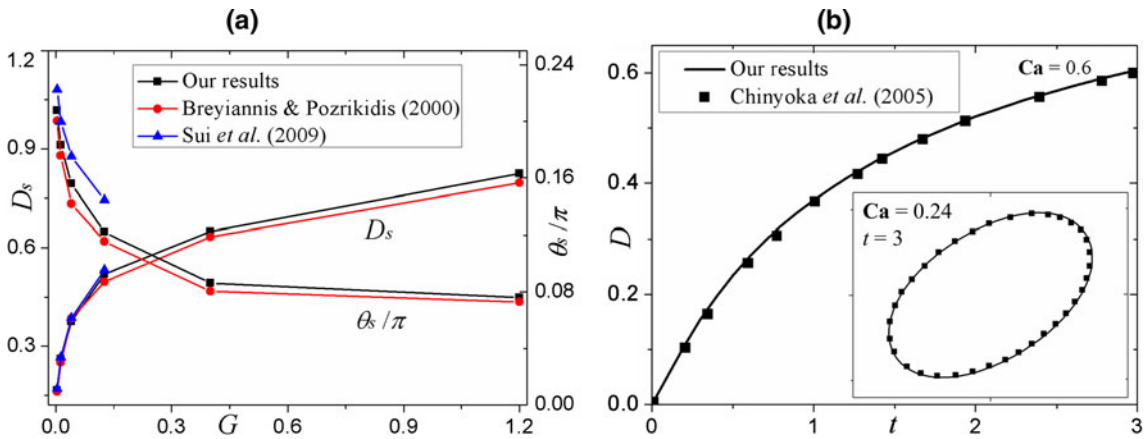

Fig. 3 Validation of our code for viscoelastic capsule deformation. **a** Comparison of steady-state deformation parameters (D and θ) for Newtonian capsules between our results and (Breyiannis and Pozrikidis 2000) and (Sui et al. 2009); **b** comparison of transient deformation D for viscoelastic drops between our results and Chinyoka's numerical results (Chinyoka et al. 2005)

3.2 Transient deformation

The transient deformation of a capsule reflects its response to the change of external fluid flow, which is common in microscale flows in vivo and in vitro. So we firstly studied the transient deforming process of a viscoelastic capsule (Fig. 4). Undershoot of the orientation angle θ and overshoot of the deformation index D were presented in our simulations, which was also observed in previous studies on the deformation of viscoelastic drops (Yue et al. 2005a). However, we found this trend of capsule transient deformation was strongly dependent upon inertia. For

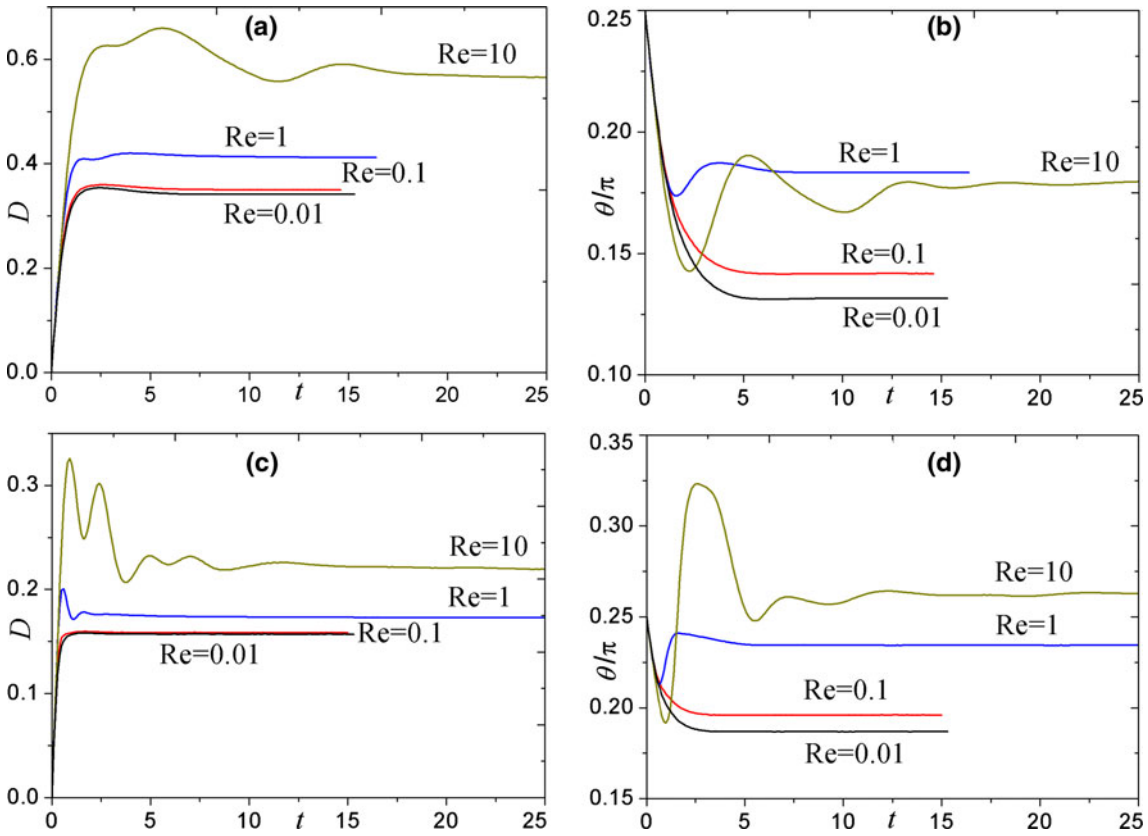

Fig. 4 Effects of inertia on transient deformation of viscoelastic capsules. **a**, **b** is temporal evolution of deformation index D and orientation angle θ for $G = 0.12$ and $De = 1.0$; **c**, **d** is temporal evolution of deformation index D and orientation angle θ for $G = 0.009375$ and $De = 1.0$

viscoelastic capsules deformed under flow conditions with low Reynolds numbers ($Re = 0.01$ and 0.1), the deformation parameters (D and θ) changed monotonically until the capsule achieved the steady state. However, as the Reynolds number was increased ($Re = 1$ and 10), damped oscillations of the deformation parameters (D and θ) were observed. Such oscillation of transient deformation was also observed in the deformation of Newtonian capsules (Sui et al. 2009) and drops (Sheth and Pozrikidis 1995; Lee and Pozrikidis 2006), only when the inertia effect was considered. As shown in our simulations, the number of oscillation cycles, oscillation time and amplitude significantly increased as the Reynolds number was increased from 1 to 10. These results indicated the transient deformation of capsules was significantly affected by inertia when Re was varied from 0.1 to 10.

To quantify the effect of inertia on the transient deformation of capsules, a steady time t_s for a viscoelastic capsule of an initially spherical shape to reach steady state was defined. The capsule deformation reached the steady state, when the difference between the transient deformation index D and its steady value D_s was less than 1 %. The steady time t_s and the error of t_s compared to its value at $Re = 0.01$ versus the Reynolds number was presented in Fig. 5. As the Reynolds number was increased from 0.01 to 10, the value of t_s significantly increased from 5.1 to 48.9 for $G = 0.12$ (and from 2.4 to 28.8 for $G = 0.009375$). However, for a capsule with dimensionless stiffness $G = 0.009375$, the steady time t_s at $Re = 0.1$ was only 4.2 % higher than that at $Re = 0.01$, while its value at $Re = 1$ was sharply increased, 108 % higher than that at $Re = 0.01$ (Fig. 5b). Similar trend for a capsule with dimensionless stiffness $G = 0.12$ was observed (Fig. 5b). These results indicated that when the Reynolds number became higher than 0.1, inertia effect on the transient deformation of viscoelastic capsules cannot be omitted due to the presence of damped oscillations, and vice versa.

3.3 Steady-state deformation

A steady state (values of D_s and θ_s remain constant) in the deformation of viscoelastic capsules was presented in our simulations (Fig. 4), consistent with previous studies on the deformation of Newtonian capsules (Eggleton and Popel 1998; Ramanujan and Pozrikidis 1998) and viscoelastic drops (Pillapakkam and Singh 2001; Yue et al. 2005b) in linear shear flow. The steady-state deformation parameters (D_s and θ_s) plotted as functions of the Deborah number De

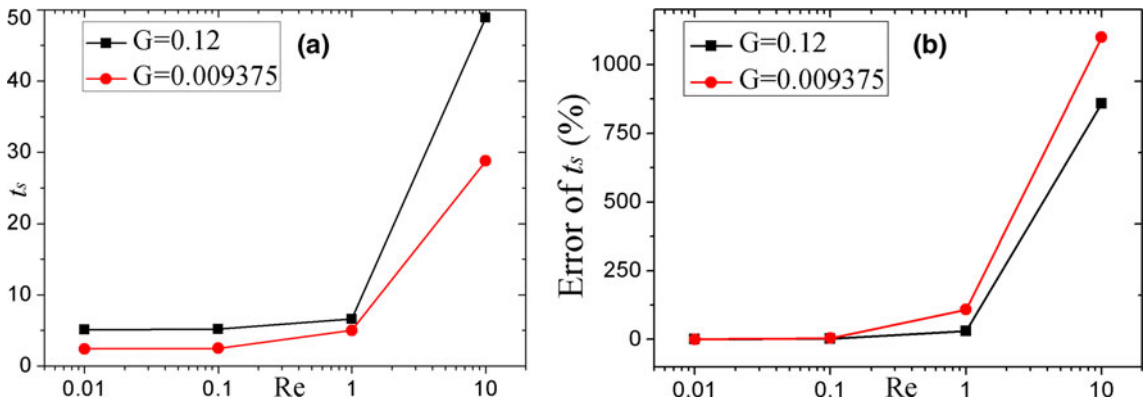

Fig. 5 Effects of inertia on the time t_s (taken for the viscoelastic capsule to reach steady state). **a** t_s versus *Re*; **b** errors of t_s compared to the value of t_s at $Re = 0.01$ ($t_s = 5.1$ for $G = 0.12$ and $t_s = 2.4$ for $G = 0.009375$) versus *Re*

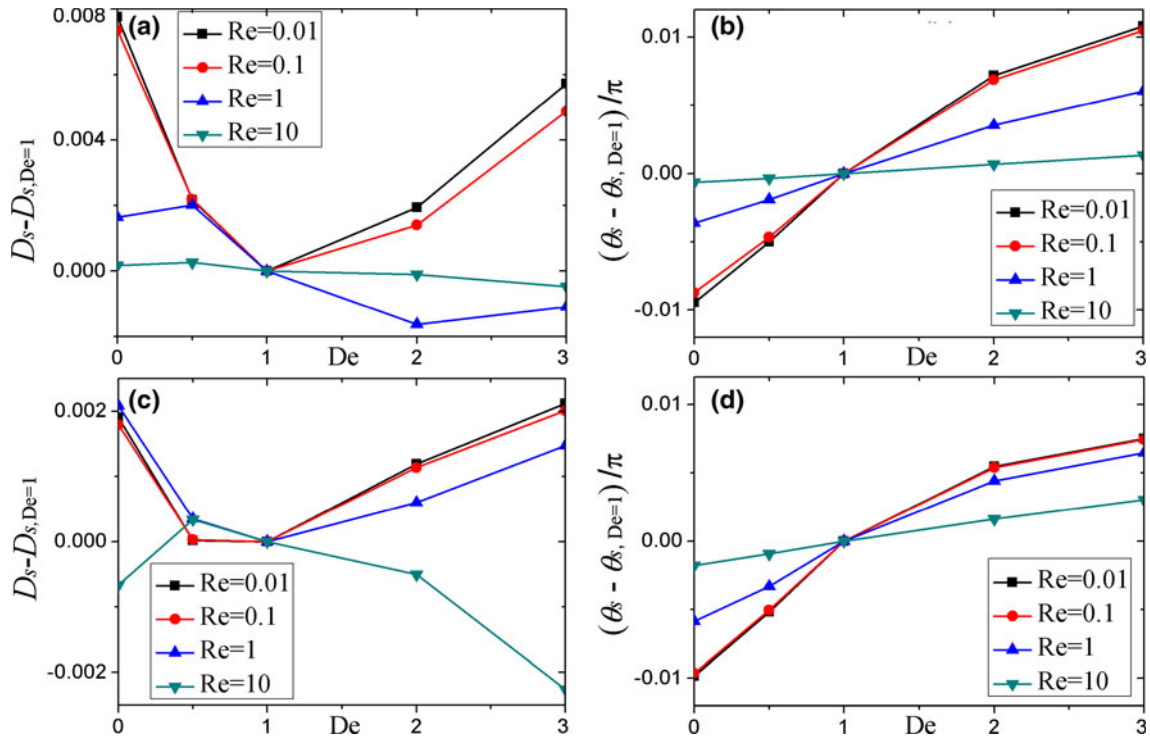

Fig. 6 Variation of steady-state deformation of viscoelastic capsules with *De* at selected Reynolds numbers. **a**, **b** is for $G = 0.009375$; **c**, **d** is for $G = 0.12$

showed the effect of fluid viscoelasticity inside capsules, at four Reynolds numbers ($Re = 0.01$, 0.1, 1 and 10) (Fig. 6). At relatively low Reynolds numbers of 0.01 and 0.1, the steady-state deformation index D_s decreased (as *De* was increased from 0 to 1) and then increased (as *De* was increased from 1 to 3), which was also observed for viscoelastic drop deformation at $Re = 0$ (Chung et al. 2008). However, when *Re* was within 1 and 10, the variation of *De* had no obvious influence on D_s (Fig. 6a, c). In comparison, the orientation angle θ_s monotonically increased with increasing *De* for all values of *Re*. It is noteworthy that the effect of *De* on θ_s increased as *Re* was reduced from 10 to 0.1, but had no significant change when *Re* was decreased further from 0.1 to 0.01. These results showed the influence of *De* on the steady-state deformation of viscoelastic capsules sharply decreased when the inertia effect became larger ($Re = 1$ and 10).

The influence of inertia upon the steady-state deformation of viscoelastic capsules was next presented, for Reynolds numbers ranging from 0.01 to 10, with the Deborah number *De* fixed at 1.0 (Fig. 7). The deformation index D_s and orientation angle θ_s sharply increased as the Reynolds number

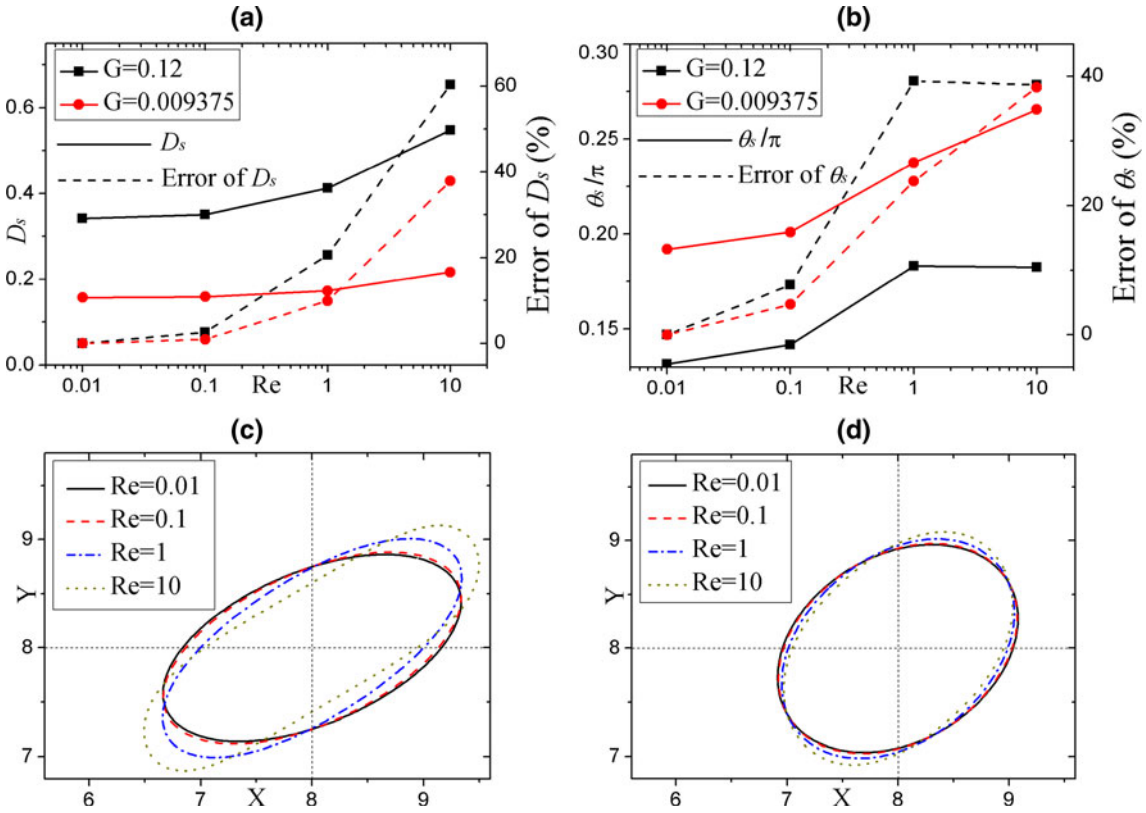

Fig. 7 Effects of inertia on steady-state deformation of viscoelastic capsules. **a**, **b** is D and θ (values and errors compared to the value at $Re = 0.01$) at steady state when $De = 1.0$; **c**, **d** is steady-state shape of initially spherical capsule at $G = 0.12$ and $G = 0.009375$ when $De = 1.0$

Re increased from 0.1 to 10, but changed little when *Re* varied in the low range, from 0.01 to 0.1. For instance, for a capsule with dimensionless stiffness $G = 0.12$, compared to the case of $Re = 0.01$, whilst the values of D_s and θ_s at $Re = 0.1$ were only 2.6 and 7.7 % larger, the corresponding values at $Re = 1$ sharply increased to 20.7 and 39.2 % larger (Fig. 7a, b). Besides, inertia significantly affected the steady-state shape of the viscoelastic capsule(Fig. 7c, d). When the Reynolds number was relatively high ($Re = 1$ and 10), both sides of the capsule became flat even concave into the capsule inside, other than convex into the capsule outside at $Re = 0.01$ and 0.1. Nevertheless, the steady-state shape of the capsule changed little when *Re* was increased from 0.01 to 0.1, maintaining the elliptical shape for all the low values of *Re* (e.g., $Re = 0.01$ and 0.1), especially for capsules with high membrane stiffness (e.g., $G = 0.009375$). These results showed that the inertia effect on the steady-state deformation of viscoelastic capsules became significant when the Reynolds number became larger than 0.1, and vice versa.

3.4 Flow structure

The kinematic structure of flow around and inside a viscoelastic capsule is essential in several research areas, e.g., shear stress distribution for the function of subcellular components, mass transport across the capsule membrane for drug delivery, and shear forces on the capsule for cell manipulation. As the Reynolds number was increased from 0.1 to 10, the flow structure inside and around the viscoelastic capsule was significantly affected by inertia (Fig. 8). Previous simulations on the deformation of Newtonian capsules (Sui et al. 2009) and drops (Sheth and Pozrikidis 1995) for Reynolds numbers ranging between 1 and 100 also revealed a strong inertia effect on flow structure. The orientation angle of the internal streamlines decreased as *Re* was increased from 0.1 to 10, which may be the reason for increasing capsule orientation angle with increasing *Re*. In addition, when *Re* became as large as 10, the streamline around the capsule exhibited bent shape instead of parallel to capsule membrane observed for smaller values of *Re* (e.g., 0.01, 0.1 and 1). This bent streamline may change the process of mass transport across the capsule membrane as well as the shear force acting on the capsule. Besides, the flow intensity inside the capsule decreased as *Re* was increased from 0.1 to 10 (Fig. 8b–d), which may decrease the magnitude of the shear stress and change its distribution inside the capsule. However, when *Re* was increased from 0.01 to 0.1, the flow structure

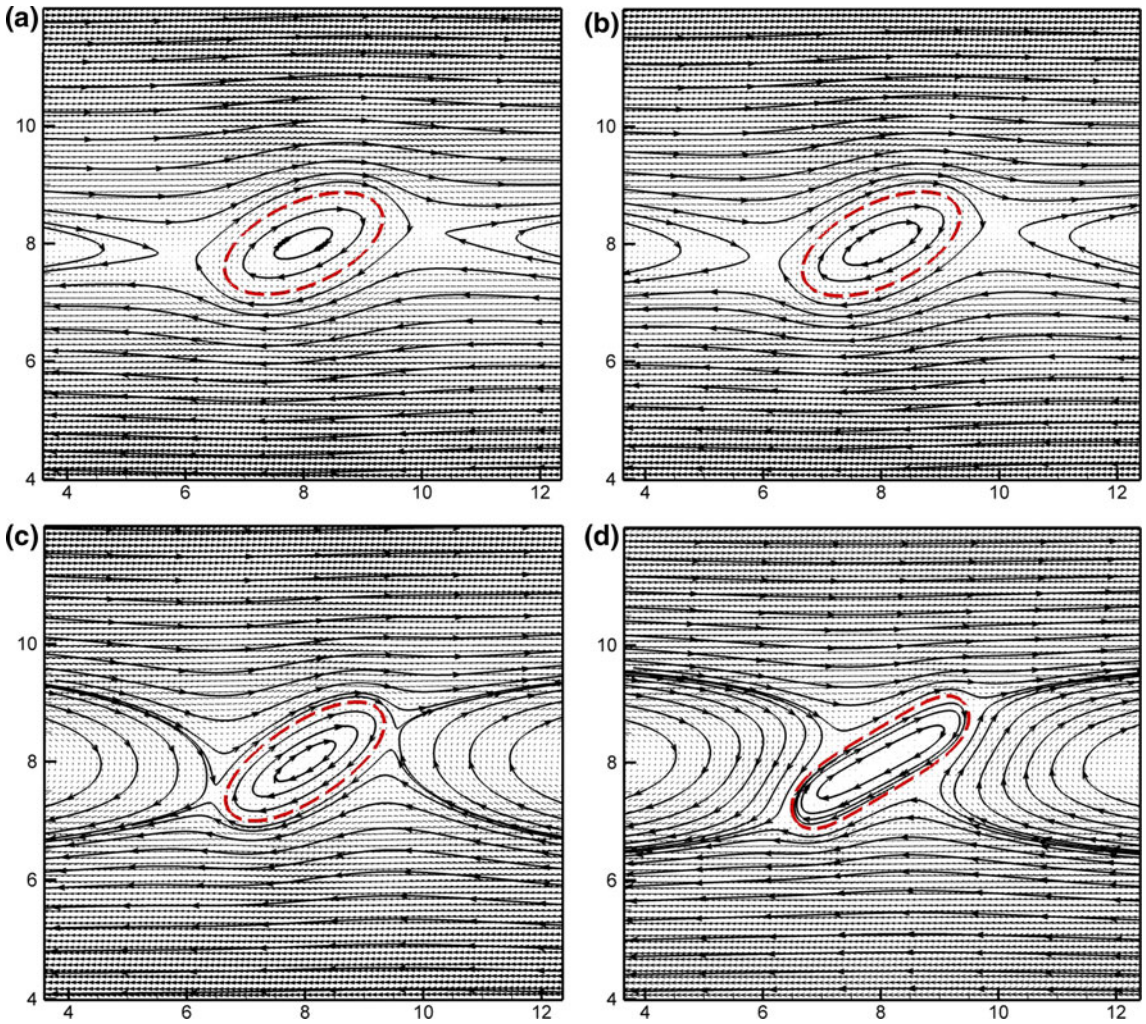

Fig. 8 Velocity vectors and stream patterns around viscoelastic capsule at steady state for $G = 0.12$ and $De = 1.0$, with *dashed line* representing capsule membrane. **a** $Re = 0.01$; **b** $Re = 0.1$; **c** $Re = 1$; **d** $Re = 10$

around and inside the capsule maintained the same pattern, and the flow intensity inside the capsule exhibited no significant change (Fig. 8a, b). These results demonstrated that the inertia effect on flow structure around and inside viscoelastic capsules cannot be neglected when the Reynolds number became higher than 0.1.

3.5 Cell deformation in microchannel

In the microcirculation, the in vivo microscale flow often happens in the microvessel with diameter less than 100 μm (Popel and Johnson 2005). The microchannel height is also typically around 100 μm in microfluidics for cell manipulation and separation (Stone and Kim 2001; Squires and Quake 2005). Thus, we studied capsule deformation in a microchannel with the height $H = 4R$ to investigate how the channel wall affects the inertia effect. Besides, material properties of actual cells (e.g., leukocytes) may be in an enormous range (Tsai et al. 1993; Chien et al. 1987), so we also investigated the inertia effect on the deformation of leukocytes in microscale flows. Parameter values for actual leukocyte deformation are listed in Table 1.

Capsule deformation was found to increase with decreasing microchannel height for Reynolds numbers ranging from 0.01 to 1, consistent with previous studies on drop deformation for $Re = 0$ (Chung et al. 2008). For example, the deformation index D_s increased from 0.34 to 0.42 as the microchannel height H was decreased from $16R$ to $4R$ for $Re = 0.01$ (Figs. 3a, 9a). Nevertheless, the inertia effect on capsule deformation in the microchannel with the height of $4R$ was still significant for Reynolds numbers ranging from 0.1 to 10, but this effect was small at low Re ($Re = 0.01$ and 0.1). For instance, compared to the case of $Re = 0.01$, whilst θ_s at $Re = 0.1$ was only 0.91 % larger, the corresponding value of θ_s at $Re = 1$ sharply increased to 9.3 % larger (Fig. 9a, b). Besides, leukocyte

Table 1 Parameter values used for leukocyte deformation in a microchannel

Parameter	Definition	Value used	References
R (μm)	Cell radius	5	(Luo et al. 2011b; Chien et al. 1987; Popel and Johnson 2005)
H (μm)	Channel height	30	(Stone and Kim 2001; Popel and Johnson 2005; Squires and Quake 2005; N'Dri et al. 2003; Pappu et al. 2008)
k (s^{-1})	Shear rate	40–40,000	(Stone and Kim 2001; Popel and Johnson 2005; Squires and Quake 2005)
ρ_0 (kg/m^3)	Extracellular fluid density	1,000	(Luo et al. 2011a, b)
μ_0 (mPa s)	Extracellular fluid viscosity	1.0	(Luo et al. 2011a, b)
ρ_1 (kg/m^3)	Cytoplasmic density	1.08	(Luo et al. 2011a, b)
μ_1 (mPa s)	Cytoplasmic viscosity	3,530	(Chien et al. 1987)
λ_1 (s)	Cytoplasmic relaxation time	0.176	(Khismatullin and Truskey 2004; Chien et al. 1987)
Eh (μN/m)	Membrane stiffness	40	(Jadhav et al. 2005; Pappu et al. 2008)

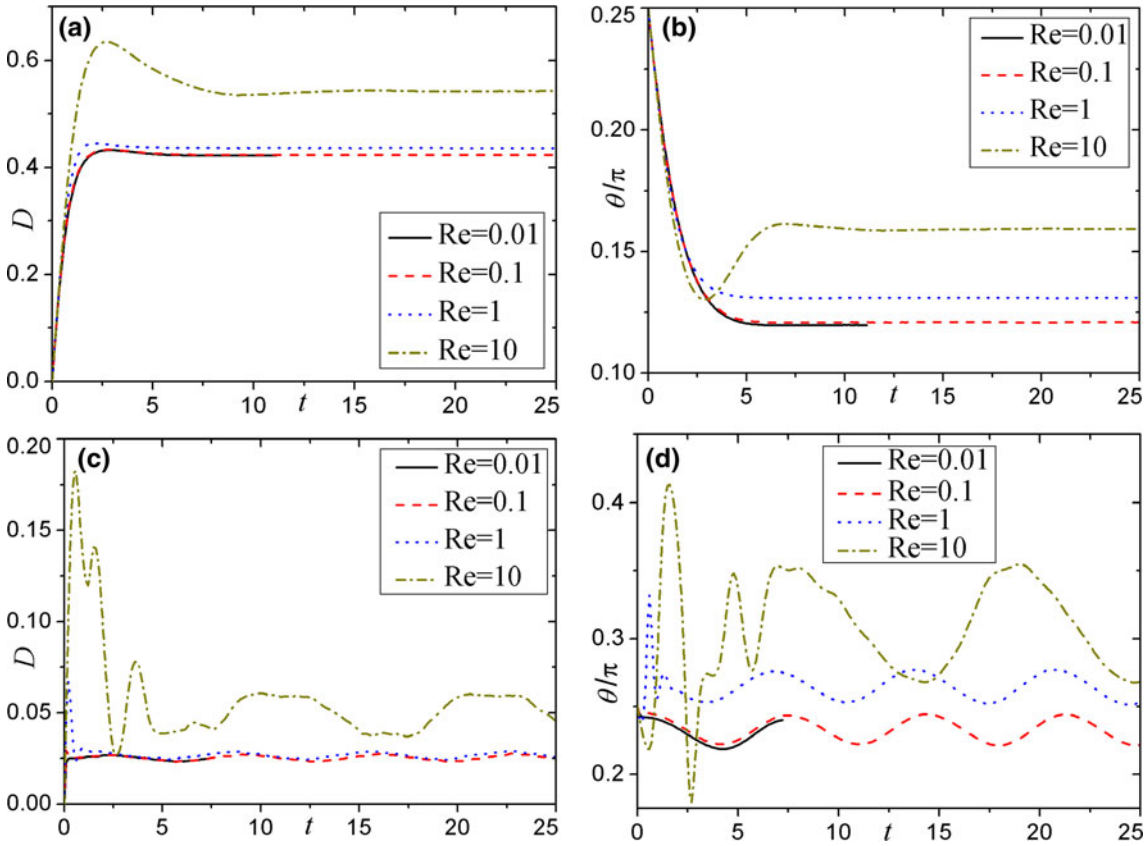

Fig. 9 Effects of inertia on the deformation of a leukocyte in microscale flows. **a**, **b** is temporal evolution of deformation index D and orientation angle θ of a capsule in a microchannel with the height of $4R$ when $G = 0.12$, $De = 0.5$; **c**, **d** is temporal evolution of deformation index D and orientation angle θ of a leukocyte in a microchannel, and parameter values used for the leukocyte is listed in Table 1

deformation in the microchannel with the height of 30 μm was also significantly affected by inertia at high Re ($Re = 0.1$ and 10), but had little change as Re was increased from 0.01 to 0.1 (Fig. 9c, d). The deformation index D_s had no significant changes (0.0240 for $Re = 0.01$ to 0.0252 for $Re = 1$) because of the high viscosity ratio ($\lambda_\mu = 3530$) of cytoplasm to plasma. However, the inclination angle θ_s significantly affected by inertia, i.e.,

compared to the case of $Re = 0.01$, the value of θ_s at $Re = 1$ was 19.0 % larger, whilst the corresponding value at $Re = 0.1$ was only 1.7 % larger. These results indicated that the inertia effect on leukocyte deformation in the microchannel cannot be omitted when the Reynolds number is higher than 0.1.

4 Discussion

By employing a finite difference-front tracking method, we established a mathematical model in which inertia was considered, and hence the inertia effect on capsule deformation in microscale flows can be investigated. A projection method based on a collocated grid system was developed to solve the full Navier–Stokes equations, which is easier to implement than previous models of capsule deformation based on a staggered grid system. Whilst Neo-Hookean constitutive law and Oldroyd-B constitutive equation were applied separately to model the elastic membrane and the internal viscoelastic fluid, other constitutive equations can be easily added into our model. To simplify the model, all the simulations were presented in a two-dimensional (2D) form which has been verified to share common features with three-dimensional (3D) simulations (Zhou and Pozrikidis 1995; Breyiannis and Pozrikidis 2000; Afkhami et al. 2009). Thus, this study greatly facilitates further theoretical modeling on microscale flows with suspending capsules in vitro and in vivo.

Our finding may provide great help to guide the selection of models for microscale flows when considering capsule deformation. To include the inertia effect on capsule deformation, the full Navier–Stokes equations that include unsteady and convective terms for inertia have to be solved. If the inertia effect on capsule deformation is negligible, the Stokes equations without unsteady and convective terms will be employed, in which we may considerably simplify the models and save the computing time. However, there is only a qualitative rule of $Re \ll 1$ in previous studies (Foessel et al. 2011; Misbah 2006; Danker et al. 2009), under which inertia can be neglected. In this study, we derived a quantitative rule of $Re < 0.1$, under which the inertia effect on capsule deformation is negligible. Thus, in further theoretical studies on microscale flows with suspending capsules, the methods neglecting inertia [e.g., boundary element method (Ramanujan and Pozrikidis 1998; Pozrikidis 2001)] may be used if $Re < 0.1$. By contrast, the methods including unsteady and convective terms in governing equations for inertia [e.g., front tracking method (Eggleton and Popel 1998; Li and Sarkar 2008; Bai et al. 2012)] are required when $Re > 0.1$.

This study may also provide great help on inertia-based microfluidic applications for cell manipulation and separation. Applications of inertial effects [e.g., inertial migration of particles (Di Carlo et al. 2007) and deformable capsules (Hur et al. 2011)] in microfluidics have been recently increasingly appreciated to develop label-free techniques, which have potential to reduce the complexity and cost of clinical microfluidic applications (Di Carlo 2009). However, the conditions (e.g., flow rate, microchannel size), under which inertial effects may be useful for cell manipulation and separation, are yet completely clear (Di Carlo et al. 2007; Di Carlo 2009). Our finding provided a quantitative guidance of $Re > 0.1$ for the design of inertia microfluidics based on capsule deformation, because inertia was found to have a little effect on capsule deformation when Re becomes less 0.1. More importantly, our model may be easily implemented to study other inertia effects on microscale flows with suspending capsules, e.g., inertial migration and ordering of capsules (Hou et al. 2010; Hur et al. 2011), inertial lift force on deformable capsules and cells (Zhao and Sharp 1999; Di Carlo 2009; Di Carlo et al. 2007). This theoretical modeling has potential to explore new system designs and to optimize the conditions for cell manipulation and separation in microfluidic devices.

It should be noted that we used the particle Reynolds number ($Re_p = \rho_0 U R^2/\mu_0 H$, including parameters for both the capsule and the microchannel flow) instead of the channel Reynolds number ($Re_c = \rho_0 U H/\mu_0$, only including parameters for the channel flow). The particle Reynolds number has been widely used in studies related to capsules suspending in flow (Di Carlo et al. 2007; Li and Sarkar 2008; Doddi and Bagchi 2008; Sui et al. 2009; Tan et al. 2012), because capsule deformation and motion are also dependent on the capsule size. We emphasize that all the simulations were focused on the deformation of single capsule in the linear shear flow, which has been greatly appreciated as being a prerequisite to that of general understanding of microscale flows with suspending capsules in vitro and in vivo (Abkarian and Viallat 2008; Di Carlo 2009). However, effects of inertia on capsule deformation and migration in parabolic flows, which is a typical flow pattern in microvessels and microfluidics, are also important and need future investigations. Besides, the cells of interest are quite dense both in physiological conditions and in vitro microfluidic applications, e.g., 1 μL of whole blood may contain millions of erythrocytes and thousands of leukocytes (Mittal et al. 2012). The collisions, aggregation and even steric interactions between these dense cells are likely to occur. The dynamic interactions between cells have significant effects on both individual cell deformation and macroscopic rheological properties. Therefore, there is an unmet need to study inertia effect on dynamic interactions between cells and to determine under which conditions this effect may be omitted. This study

provides a model which could be further developed to study inertia effect on dynamic interactions of suspending cells in microscale flows.

5 Conclusion

We developed a mathematical model considering inertia in microscale flows. Using this model, we investigated the inertia effect on the deformation of viscoelastic capsules in microscale flows with the Reynolds numbers varying in the physiological range of 0.01–10. It was demonstrated that, when the Reynolds number was increased from 0.1 to 10, inertia significantly affected several important features of capsule deformation including: (1) rapid increase in the time and amplitude of the transient deformation; (2) significant enhancement in the deformation index and orientation angle of the capsule in steady state; (3) considerable alteration of the flow structure around and inside the capsule. However, all these features of capsule deformation exhibited no significant change when the Reynolds number was varied between 0.01 and 0.1. These results revealed that the inertia effect on viscoelastic capsule deformation in microscale flows may be neglected when Reynolds numbers is smaller than 0.1. Our findings are beneficial to further study both the mechanism of biological processes and the design of microfluidic devices for bioengineering applications, when inertial effects in microscale flows are involved.

Acknowledgments This work was supported by the Specialized Research Fund for the Doctoral Program of Higher Education of China (20110201110029). This research was partially supported by the Foundation for Innovative Research Groups of the National Natural Science Foundation of China (Grant No. 50821064); the Major International (Regional) Joint Research Program of China (11120101002); National Natural Science Foundation of China (10825210, 31050110125); and the National 111 Project of China (B06024).

References

Abkarian M, Viallat A (2008) Vesicles and red blood cells in shear flow. Soft Matter 4(4):653–657. doi:10.1039/b716612e

Afkhami S, Yue P, Renardy Y (2009) A comparison of viscoelastic stress wakes for two-dimensional and three-dimensional Newtonian drop deformations in a viscoelastic matrix under shear. Physics Fluids 21(7). doi:10.1063/1.3182830

Bagchi P (2007) Mesoscale simulation of blood flow in small vessels. Biophys J 92(6):1858–1877. doi:10.1529/biophysj.106.095042

Bagchi P, Johnson PC, Popel AS (2005) Computational fluid dynamic simulation of aggregation of deformable cells in a shear flow. J Biomech Eng Trans ASME 127(7):1070–1080. doi:10.1115/1.2112907

Bai BF, Luo ZY, Lu TJ, Xu F (2012) Numerical simulation of cell adhesion and detachment in microfluidics. J Mech Med Biol 1350002. doi:10.1142/S0219519413500024

Beech JP, Holm SH, Adolfsson K, Tegenfeldt JO (2012) Sorting cells by size, shape and deformability. Lab Chip 12(6):1048–1051. doi:10.1039/c2lc21083e

Bird RB, Wiest JM (1995) Constitutive equations for polymeric fluid. Annu Rev Fluid Mech 27:169–193. doi:10.1146/annurev.fluid.27.1.169

Boger DV (1977) Highly elastic constant-viscosity fluid. J Non Newton Fluid Mech 3(1):87–91. doi:10.1016/0377-0257(77)80014-1

Breyiannis G, Pozrikidis C (2000) Simple shear flow of suspensions of elastic capsules. Theor Comput Fluid Dyn 13(5):327–347. doi:10.1007/s001620050003

Chien S, Sung KLP, Schmidschonbein GW, Skalak R, Schmalzer EA, Usami S (1987) Rheology of Leukocytes. Ann N Y Acad Sci 516:333–347. doi:10.1111/j.1749-6632.1987.tb33054.x

Chinyoka T, Renardy YY, Renardy A, Khismatullin DB (2005) Two-dimensional study of drop deformation under simple shear for Oldroyd-B liquids. J Non Newton Fluid Mech 130(1):45–56. doi:10.1016/j.jnnfm.2005.07.005

Chung C, Hulsen MA, Kim JM, Ahn KH, Lee SJ (2008) Numerical study on the effect of viscoelasticity on drop deformation in simple shear and 5:1:5 planar contraction/expansion microchannel. J Non Newton Fluid Mech 155(1–2):80–93. doi:10.1016/j.jnnfm.2008.06.002

Danker G, Vlahovska PM, Misbah C (2009) Vesicles in Poiseuille Flow. Phys Rev Lett 102(14):4. doi:10.1103/PhysRevLett.102.148102

Di Carlo D (2009) Inertial microfluidics. Lab Chip 9(21):3038–3046. doi:10.1039/b912547g

Di Carlo D, Irimia D, Tompkins RG, Toner M (2007) Continuous inertial focusing, ordering, and separation of particles in microchannels. Proc Natl Acad Sci USA 104(48):18892–18897. doi:10.1073/pnas.0704958104

Didar TF, Tabrizian M (2010) Adhesion based detection, sorting and enrichment of cells in microfluidic Lab-on-Chip devices. Lab Chip 10(22):3043–3053. doi:10.1039/c0lc00130a

Doddi SK, Bagchi P (2008) Effect of inertia on the hydrodynamic interaction between two liquid capsules in simple shear flow. Int J Multiph Flow 34(4):375–392. doi:10.1016/j.ijmultiphaseflow.2007.10.011

Dong C, Cao J, Struble EJ, Lipowsky HW (1999) Mechanics of leukocyte deformation and adhesion to endothelium in shear flow. Ann Biomed Eng 27(3):298–312. doi:10.1114/1.143

Eggleton CD, Popel AS (1998) Large deformation of red blood cell ghosts in a simple shear flow. Phys Fluids 10(8):1834–1845. doi:10.1063/1.869703

Foessel E, Walter J, Salsac AV, Barthes-Biesel D (2011) Influence of internal viscosity on the large deformation and buckling of a spherical capsule in a simple shear flow. J Fluid Mech 672:477–486. doi:10.1017/s0022112011000280

Hou HW, Bhagat AAS, Chong AGL, Mao P, Tan KSW, Han JY, Lim CT (2010) Deformability based cell margination-A simple microfluidic design for malaria-infected erythrocyte separation. Lab Chip 10(19):2605–2613. doi:10.1039/c003873c

Hur SC, Henderson-MacLennan NK, McCabe ERB, Di Carlo D (2011) Deformability-based cell classification and enrichment using inertial microfluidics. Lab Chip 11(5):912–920. doi:10.1039/c0lc00595a

Jadhav S, Eggleton CD, Konstantopoulos K (2005) A 3-D computational model predicts that cell deformation affects selectin-mediated leukocyte rolling. Biophys J 88(1):96–104. doi:10.1529/biophysj.104.051029

Khismatullin DB, Truskey GA (2004) A 3D numerical study of the effect of channel height on leukocyte deformation and adhesion in parallel-plate flow chambers. Microvasc Res 68(3):188–202. doi:10.1016/j.mvr.2004.07.003

Lac E, Barthes-Biesel D (2005) Deformation of a capsule in simple shear flow: effect of membrane prestress. Phys Fluids 17(7):8. doi:10.1063/1.1955127

Lauga E, Brenner MP, Stone HA (2007) Microfluidics: the no-slip boundary condition. In: Tropea C, Yarin A, Foss JF (eds) Handbook of experimental fluid dynamics. Springer, Berlin

Lee J, Pozrikidis C (2006) Effect of surfactants on the deformation of drops and bubbles in Navier–Stokes flow. Comput Fluids 35(1):43–60. doi:10.1016/j.compfluid.2004.11.004

Ley K, Laudanna C, Cybulsky MI, Nourshargh S (2007) Getting to the site of inflammation: the leukocyte adhesion cascade updated. Nat Rev Immunol 7(9):678–689. doi:10.1038/nri2156

Li XY, Sarkar K (2008) Front tracking simulation of deformation and buckling instability of a liquid capsule enclosed by an elastic membrane. J Comput Phys 227(10):4998–5018. doi:10.1016/j.jcp.2008.01.034

Luo ZY, Xu F, Lu TJ, Bai BF (2011a) Direct numerical simulation of detachment of single captured leukocyte under different flow conditions. J Mech Med Biol 11(2):273–284. doi:10.1142/s0219519411004034

Luo ZY, Xu F, Lu TJ, Bai BF (2011b) Direct numerical simulation of single leukocyte deformation in microchannel flow for disease diagnosis. J Med Syst 35(5):869–876. doi:10.1007/s10916-010-9502-3

McWhirter JL, Noguchi H, Gompper G (2009) Flow-induced clustering and alignment of vesicles and red blood cells in microcapillaries. Proc Natl Acad Sci USA 106(15):6039–6043. doi:10.1073/pnas.0811484106

Misbah C (2006) Vacillating breathing and tumbling of vesicles under shear flow. Phys Rev Lett 96(2):4. doi:10.1103/PhysRevLett.96.028104

Mittal S, Wong IY, Deen WM, Toner M (2012) Antibody-functionalized fluid-permeable surfaces for rolling cell capture at high flow rates. Biophys J 102(4):721–730. doi:10.1016/j.bpj.2011.12.044

N'Dri NA, Shyy W, Tran-Soy-Tay R (2003) Computational modeling of cell adhesion and movement using a continuum-kinetics approach. Biophys J 85:2273–2286. doi:10.1016/S0006-3495(03)74652-9

Pappu V, Doddi SK, Bagchi P (2008) A computational study of leukocyte adhesion and its effect on flow pattern in microvessels. J Theor Biol 254(2):483–498. doi:10.1016/j.jtbi.2008.05.020

Peskin CS (1977) Numerical analysis of blood flow in the heart. J Comput Phys 25(3):220–252. doi:10.1016/0021-9991(77)90100-0

Pillapakkam SB, Singh P (2001) A level-set method for computing solutions to viscoelastic two-phase flow. J Comput Phys 174(2):552–578. doi:10.1006/jcph.2001.6927

Popel AS, Johnson PC (2005) Microcirculation and hemorheology. Annu Rev Fluid Mech 37:43–69. doi:10.1146/annurev.fluid.37.042604.133933

Pozrikidis C (2001) Effect of membrane bending stiffness on the deformation of capsules in simple shear flow. J Fluid Mech 440:269–291

Ramanujan S, Pozrikidis C (1998) Deformation of liquid capsules enclosed by elastic membranes in simple shear flow: large deformations and the effect of fluid viscosities. J Fluid Mech 361:117–143. doi:10.1017/S0022112098008714

Sarkar K, Schowalter WR (2000) Deformation of a two-dimensional viscoelastic drop at non-zero Reynolds number in time-periodic extensional flows. J Non Newton Fluid Mech 95(2–3):315–342. doi:10.1016/s0377-0257(00)00156-7

Sheth KS, Pozrikidis C (1995) Effects of inertia on the deformation of liquid drops in simple shear flow. Comput Fluids 24(2):101–119. doi:10.1016/0045-7930(94)00025-t

Squires TM, Quake SR (2005) Microfluidics: fluid physics at the nanoliter scale. Rev Mod Phys 77(3):977–1026. doi:10.1103/RevModPhys.77.977

Stone HA, Kim S (2001) Microfluidics: basic issues, applications, and challenges. AIChE J 47(6):1250–1254. doi:10.1002/aic.690470602

Sui Y, Chew YT, Low HT (2007) A lattice Boltzmann study on the large deformation of red blood cells in shear flow. Int J Mod Phys C 18(6):993–1011. doi:10.1142/s012918310701108x

Sui Y, Chew YT, Roy P, Low HT (2009) Inertia effect on the transient deformation of elastic capsules in simple shear flow. Comput Fluids 38(1):49–59. doi:10.1016/j.compfluid.2007.11.006

Tan MHY, Le DV, Chiam KH (2012) Hydrodynamic diffusion of a suspension of elastic capsules in bounded simple shear flow. Soft Matter 8(7):2243–2251. doi:10.1039/c2sm06496k

Tryggvason G, Bunner B, Esmaeeli A, Juric D, Al-Rawahi N, Tauber W, Han J, Nas S, Jan YJ (2001) A front-tracking method for the computations of multiphase flow. J Comput Phys 169(2):708–759. doi:10.1006/jcph.2001.6726

Tsai MA, Frank RS, Waugh RE (1993) Passive mechanical behavior of human neutrophils: power-law fluid. Biophys J 65(5):2078–2088

Unverdi SO, Tryggvason G (1992) A front-tracking method for viscous, incompressible, multi-fluid flows. J Comput Phys 100(1):25–37. doi:10.1016/0021-9991(92)90307-K

Worner M (2012) Numerical modeling of multiphase flows in microfluidics and micro process engineering: a review of methods and applications. Microfluid Nanofluid 12(6):841–886. doi:10.1007/s10404-012-0940-8

Wu ZG, Willing B, Bjerketorp J, Jansson JK, Hjort K (2009) Soft inertial microfluidics for high throughput separation of bacteria from human blood cells. Lab Chip 9(9):1193–1199. doi:10.1039/b817611f

Yue P, Feng JJ, Liu C, Shen J (2005a) Transient drop deformation upon startup of shear in viscoelastic fluids. Phys Fluids 17 (12). doi:10.1063/1.2139630

Yue PT, Feng JJ, Liu C, Shen J (2005b) Viscoelastic effects on drop deformation in steady shear. J Fluid Mech 540:427–437. doi:10.1017/s0022112005006166

Zhao Y, Sharp MK (1999) Finite element analysis of the lift on a slightly deformable and freely rotating and translating cylinder in two-dimensional channel flow. J Biomech Eng Trans ASME 121(2):148–152. doi:10.1115/1.2835096

Zhou H, Pozrikidis C (1995) Deformation of liquid capsules with incompressible interfaces in simple shear flow. J Fluid MECH 283:175–200. doi:10.1017/s0022112095002278